ARL-TR-9120 ● Dec 2020

DEVCOM ARMY RESEARCH LABORATORY

# Compression Strength of Borosilicate and Soda-Lime Silicate Glasses Using a Dumbbell-Shaped Specimen

by Christopher S Meredith and Jeffrey J Swab

## NOTICES

### Disclaimers

The findings in this report are not to be construed as an official Department of the Army position unless so designated by other authorized documents.

Citation of manufacturer's or trade names does not constitute an official endorsement or approval of the use thereof.

Destroy this report when it is no longer needed. Do not return it to the originator.

ARL-TR-9120 ● DEC 2020


# Compression Strength of Borosilicate and Soda-Lime Silicate Glasses Using a Dumbbell-Shaped Specimen

**Christopher S Meredith and Jeffrey J Swab**
***Weapons & Materials Research Directorate, DEVCOM Army Research Laboratory***

# REPORT DOCUMENTATION PAGE

*Form Approved*
*OMB No. 0704-0188*



| 1. REPORT DATE *(DD-MM-YYYY)* | 2. REPORT TYPE | 3. DATES COVERED (From - To) |
|---|---|---|
| December 2020 | Technical Report | January 2018–June 2020 |

**4. TITLE AND SUBTITLE**
Compression Strength of Borosilicate and Soda-Lime Silicate Glasses Using a Dumbbell-Shaped Specimen

**5a. CONTRACT NUMBER**

**5b. GRANT NUMBER**

**5c. PROGRAM ELEMENT NUMBER**

**6. AUTHOR(S)**
Christopher S Meredith and Jeffrey J Swab

**5d. PROJECT NUMBER**

**5e. TASK NUMBER**

**5f. WORK UNIT NUMBER**

**7. PERFORMING ORGANIZATION NAME(S) AND ADDRESS(ES)**
DEVCOM Army Research Laboratory
ATTN: FCDD-RLW-PC
Aberdeen Proving Ground, MD 21005

**8. PERFORMING ORGANIZATION REPORT NUMBER**
ARL-TR-9120

**9. SPONSORING/MONITORING AGENCY NAME(S) AND ADDRESS(ES)**

**10. SPONSOR/MONITOR'S ACRONYM(S)**

**11. SPONSOR/MONITOR'S REPORT NUMBER(S)**

**12. DISTRIBUTION/AVAILABILITY STATEMENT**
Approved for public release; distribution is unlimited.

**13. SUPPLEMENTARY NOTES**
ORCID IDs: Christopher S Meredith, 0000-0003-1368-8003; Jeffrey J Swab, 0000-0002-8204-7202

**14. ABSTRACT**

The compression strength of a borosilicate and a soda-lime silicate glass is measured under quasi-static and dynamic strain rates with a dumbbell-shaped specimen. Two different specimen orientations were machined, parallel (vertical) and perpendicular (horizontal) to the plate thickness, and some specimens of each glass were etched prior to testing. A dumbbell specimen was used since the typical cuboid or cylindrical specimen develops a large stress concentration at the ends of the specimen, leading to premature failure and correspondingly low strength values. The dumbbell-shaped specimen allows one to differentiate between "valid" and "invalid" failure for each experiment by observing, with a high-speed camera, where fracture initiates—within the specimen gage section (valid) or from the specimen ends (invalid). However, damage can initiate in both the ends and the gage section (nearly) simultaneously, clouding the determination. Time correlating the force/stress measurement to the observed images has some uncertainty that can add additional ambiguity. The success rates for each glass were completely opposite: relatively high for borosilicate and very low for the soda-lime silicate. However, there is no obvious explanation. Despite these issues, it is believed that the dumbbell-shaped specimen is the best geometry for measuring the compression strength of brittle materials.

**15. SUBJECT TERMS**
soda-lime silicate glass, borosilicate glass, dumbbell-shaped specimen, compression strength, split-Hopkinson pressure (Kolsky) bar, brittle fracture

| 16. SECURITY CLASSIFICATION OF: | | | 17. LIMITATION OF ABSTRACT | 18. NUMBER OF PAGES | 19a. NAME OF RESPONSIBLE PERSON |
|---|---|---|---|---|---|
| a. REPORT | b. ABSTRACT | c. THIS PAGE | | | Christopher S Meredith |
| Unclassified | Unclassified | Unclassified | UU | 34 | 19b. TELEPHONE NUMBER (Include area code) (410) 278-6715 |

## Contents

## List of Figures



## List of Tables

## Acknowledgments

Thanks to Kevin Taylor, who helped with performing the Kolsky bar experiments, and Steve Kilczewski and Victoria Blair, who performed the hydrofluoric treatments.

# 1. Introduction

Glass is a critical strike-face component of many transparent armor systems. The glass typically used in these systems is produced by the float process, where a glass sheet is made by floating molten glass on a bed of molten tin. This process yields large and inexpensive glass sheets having a uniform thickness and very flat surfaces. Much of this glass is used commercially as architectural and optical windows, and the glass in commercial displays and mirrors are made by this process. Chemical and/or thermal treatments can be applied to make the glass stronger and more scratch-resistant for use in automobile windshields, as well as in computer, television, and phone screens. Soda-lime silicate is the most prevalent glass used in the world. It is relatively cheap and can be manufactured and processed at lower temperatures. It is composed mainly of silicon dioxide, sodium oxide, and calcium oxide. Soda-lime silicate is the glass most commonly used for window panes and drinking glasses as well as bottles and jars used for food storage. Borosilicate glass consists mainly of silicon dioxide, boric oxide, sodium oxide, and aluminum oxide. It has a very low coefficient of thermal expansion, resulting in lower susceptibility to thermal shock. Additionally, it is also less dense and more abrasion- and chemical-resistant than soda-lime silicate, but the increased manufacturing and processing temperatures required increase the cost. Borosilicate glass is the preferred glass for laboratory glassware, medical vials, and syringes as well as many common pieces of household bake and cookware.

Float glass can be easily cut into a variety of prismatic shapes, so flexure strength is a commonly determined mechanical property. Prismatic beam specimens can readily be made for four-point flexure testing according to ASTM C158-02,[1] while large square or rectangular plates can be used in equibiaxial flexure testing. Unfortunately, there is no ASTM standard in place for equibiaxial flexure testing of glass, but the general procedures and test methodology outlined in ASTM C1499-09[2] have been successfully modified and applied to borosilicate and soda-lime silicate float glasses.[3–5] This method of flexure strength testing is finding favor in the ceramics and glass communities. Because of the equibiaxial stress state created, the larger amount of material interrogated during loading compared with four-point flexure and the influence of the specimen edges—specifically, the quality of these edges—can be minimized.

While flexure strength is an important glass property, another strength value—compression strength—is important for transparent armor applications since a compressive stress is created during the initial stages of a ballistic event. Unfortunately, the compressive strength of glass is not typically determined. A review of the literature shows surprising few studies in this area. Work by

Bridgman during the 1930s through 1950s was focused on confined compression strength[6–8] with virtually no compression strength values being reported. In the late 1960s, Outwater and Gerry tested "necked down" Pyrex rods and reported a maximum compression around 3.8 GPa.[9,10] They observed triboluminescence above 3.2 GPa and a change in fracture morphology around 3 GPa. Below 3 GPa, the rod would "splinter", while above this value, the rod would deform, resulting in the formation of a "white coherent mass".

In 1969, Ernsberger[11] used a unique method to create an internal oblate bubble in cylindrical specimens of soda-lime silicate, Pyrex, and fused silica to determine the tensile and compressive strength of each glass. He was interested in obtaining the strength of a "pristine" glass and assumed that the internal bubble was free of flaws and environmental effects. The specimen was placed in tension, which created a compressive stress on the bubble walls, with the maximum stress occurring at the bubble tip. The soda-lime silicate fractured due to shear bands that developed at the tip, while both the Pyrex and fused silica did not fail. Instead, densification was observed at the tip in both of these glasses. Ernsberger reported an intrinsic compressive strength between 4.2 and 4.5 GPa for the soda-lime silicate glass. The stresses required for densification to occur in the Pyrex and fused silica where approximately 7.6 and 9.1 GPa, respectively. A year later, the strength of a glass cylinder, quasi-statically loaded between two platens, was reported to be between 0.55 and 1.9 GPa.[12]

Almost four decades passed before a series of papers were published by a group from Southwest Research Institute.[13–16] In all of these studies, they examined cylindrical specimens of a borosilicate (BOROFLOAT 33[*]) and a soda-lime silicate (Starfire[†]) float glass being considered for transparent armor applications. Most of the tests were conducted with the specimens under various states of confinement and either under quasi-static or dynamic loading ($10^2$/s) using a split-Hopkinson pressure bar (Kolsky bar). A few specimens were conducted without any confinement, and some were "damaged" by exposing the specimens to a thermal shock cycle prior to testing. The purpose was to identify the strength behavior of the confined glass, both intact and damaged, and to identify the parameters for the modeling and simulation tools used to predict ballistic performance. The unconfined equivalent stress of the BOROFLOAT 33 ranged between 1.4 and 2.6 GPa,[14] and the unconfined equivalent stress of the Starfire was between 1.3 and

[*] BOROFLOAT 33, Schott North America, Duryea, Pennsylvania

[†] Starphire, PPG Industries, Inc, Pittsburgh, Pennsylvania

2.2 GPa,[16] but in both cases, these ranges were determined using only three specimens for each glass.

Over the ensuing years, others have also measured the compression strength of glasses, but there has been significant variability in the data reported. A group in Europe reported the quasi-static and dynamic strength of an unidentified glass was 1–1.2 GPa,[17] while a group in Asia[18] conducted similar tests on an annealed float glass and reported a quasi-static compression strength around 250 MPa, while the dynamic strength ranged from 300 to 800 MPa. Daryadel et al.[19] conducted tests at strain rates of 70/s and 375/s on four glasses: a soda-lime silicate, Starphire, BOROFLOAT 33, and fused silica. The compression strength was essentially the same for all four glasses at 70/s (~400 MPa) and it increased for all the glasses to between 825 and 950 MPa at 375/s. Nie et al.[20] used cuboid specimens of a borosilicate float glass that had two parallel end-faces machined at angles of 0°, 3°, 5°, and 7° to introduce a shear stress using a split-Hopkinson pressure bar unit. The stress at the time of damage initiation in the 0° specimens averaged 1.3 GPa. This stress decreased with increasing face angle to a low of 560 MPa for the specimen with the 7° tilt.

The purpose of this report is to determine the quasi-static and dynamic compression strength of a soda-lime silicate glass and a borosilicate float glass that are being considered for transparent armor applications. In these tests, a dumbbell-shaped specimen, Fig. 1, was used instead of the typical cylindrical or cuboidal specimen. The dumbbell specimen was designed by Tracy et al.[21,22] in the 1980s to promote fracture occurring in the gage section and has been successfully used to determine the quasi-static compressive strength of various advanced ceramics over the years.[23–25] A recent round-robin exercise showed that this specimen can be successfully used in a Kolsky bar to determine the dynamic compression strength of alumina.[26]

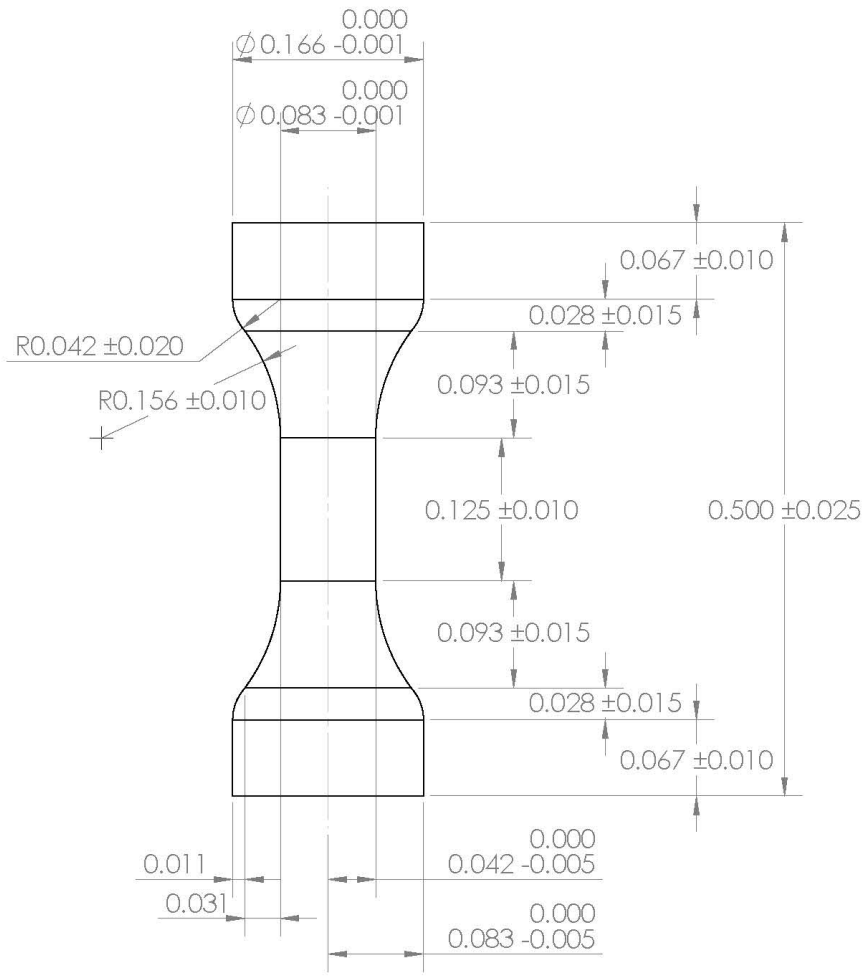


**Fig. 1 Dumbbell-shaped specimen; all units in inches**

## 2. Materials

The two glasses studied in this effort were a borosilicate (BOROFLOAT 33, from Schott North America, Duryea, Pennsylvania) and a soda-lime silicate (Starphire, from PPG Industries, Inc, Pittsburgh, Pennsylvania). Typical properties of these glasses can be found on the respective company websites and in Weresczcak and Anderson.[27] The dimensions of the dumbbell-shaped specimens are given in Fig. 1. All specimens were cut from a single 1-inch-thick plate of each glass using conventional diamond grinding. This specimen is a scaled-down version of the specimens originally developed by Tracy et al.[21–23] and described in ASTM C1424-15.[28] Two orientations for each glass were machined, one where the specimen long axis was perpendicular to the plate thickness ("horizontal" direction) and the second where this axis is parallel to it ("vertical" direction). This was done in an attempt to determine if a strength anisotropy existed in these glasses. Prior to testing, some of the samples were etched with hydrofluoric acid (HF) solution in an attempt to

reduce surface damage from the machining process. The Starphire was etched for 1.5 min in a 20-mole% HF solution, while the BOROFLOAT 33 was etched for 5 min in a 10–20 mole% HF solution. After etching, the samples were immediately stored in containers with an argon atmosphere to minimize any environmental effects prior to testing.

## 3. Experimental Procedures

Quasi-static testing was performed according to guidelines and procedures in ASTM C1424-15[28] using a universal load frame at a displacement rate of 0.5 mm/min. The specimen was placed between sacrificial tungsten carbide (WC) load blocks to minimize any damage to the steel loading platens. A preload of no more than 500 N was applied to the specimen to check alignment prior to testing. The failure process of each specimen was recorded using a Photron SA1 camera with a 105-mm lens at 75,000 frames/s to determine if fracture initiated in the gage section of the specimen (valid test) or the end of the specimen (invalid test).

Dynamic, high-strain-rate testing was conducted with a Kolsky bar using the same dumbbell-shaped specimen used in the quasi-static tests. The bars that comprised the split-Hopkinson pressure bar unit were 6.35 mm in diameter and made of maraging steel C350. The lengths of the incident and transmitted bars were 914 mm, and striker bar was 76 mm long. The pulse shaper was a stamped-out disk of aluminum 1100 sheet with a nominal diameter of 3.1 mm and a thickness of 0.15 mm.

The usual way of calculating the specimen strain with the Kolsky bar is to integrate the reflected wave; however, with the dumbbell-shaped specimens, a significant amount of strain develops outside of the gage section that would be part of the strain measurement. Therefore, this method was not used to measure strain. In our previous work testing this geometry on boron carbide ($B_4C$),[25] a strain gage was attached to the gage section of the specimen to measure strain. Because glass is particularly sensitive to surface flaws that can influence the strength, we were not planning on mounting strain gages to the specimens. However, after observing the quasi-static results, where there was no difference in strength between etched and unetched borosilicate glass, we chose to mount them only onto the unetched borosilicate. The surface preparation procedure for “glass” in Vishay Precision Group’s Instruction Bulletin B-129-8[29] was followed, whereby the sample surface was only cleaned; no abrading of the surface was performed. Kyowa KFRS-02-120-C1 strain gages were adhered using Vishay Precision Group’s M-Bond AE-10 epoxy. However, gage application proved to be unsuccessful because the gages mostly came off during dynamic loading prior to failure or prior

to testing. As a result, stress as a function of time is plotted in this report. When testing brittle materials with the Kolsky bar, WC platens placed on either side of the sample are routinely used; however, they were not used in this study for three reasons. First, impedance-matching the WC to the chosen steel bars would have resulted in the WC platens being a smaller diameter than the ends of the specimen. Second, from our previous work on $B_4C$, where we also did not use WC platens, we had an approximately 44% valid test rate. Since $B_4C$ is significantly stronger than glass, we expected a higher success rate due to a reduction in the stress concentration between the bars and specimen. And third, adding WC platens results in undesirable wave reflections that can increase the noise and uncertainty of the measurement. The dumbbell shape already adds reflections due to the changes in diameter associated with the geometry. Since the stress measurement is already indirect, adding platens makes it even more so.

Finally, there was a large diameter mismatch between the bars and sample, so polycarbonate alignment collets were machined that aligned them coaxially (see Swab et al.[25]). This ensured each test had very good and consistent alignment. To confirm the validity of each test, a Shimadzu HPV-X2 high-speed camera recorded the specimen fracture at between 1 and 5 million frames/s. The camera and strain gage recording on the bars shared a common trigger so that the individual images could be time-correlated to the stress measurement.

## 4. Results

**Quasi-static testing.** Table 1 summarizes the quasi-static results from this study. Fifteen of the 17 tests on the borosilicate glass were valid (fracture initiated in the specimen gage section), and there is no statically significant strength difference as a function of specimen orientation or whether the specimen was etched or not. The compression strength in the horizontal and vertical directions is 1.4 ± 0.1 and 1.3 ± 0.0 GPa, respectively, for the unetched specimens, and 1.5 ± 0.3 GPa for the etched specimens in the horizontal direction (no vertical direction specimens were etched). Based on these results it appears that the HF etching was ineffective in reducing the size and number of surface flaws.

**Table 1 Quasi-static compression strength results for borosilicate and soda-lime silicate glasses**

| Material | Direction | Unetched | | | | HF-etched | | | |
|---|---|---|---|---|---|---|---|---|---|
| | | $\sigma_c$ (GPa) | StD | No. Specimens | Valid | $\sigma_c$ (GPa) | StD | No. Specimens | Valid |
| Borosilicate glass | Horizontal | 1.4 | 0.1 | 6 | 5 | 1.5 | 0.3 | 8 | 7 |
| | Vertical | 1.3 | 0.0 | 5 | 5 | . . . | . . . | . . . | . . . |
| Soda-lime glass | Horizontal | 1.7 | 0.0 | 8 | 2 | . . . | . . . | 6 | 0 |
| | Vertical | 1.7 | . . . | 4 | 1 | . . . | . . . | 4 | 0 |

The success rate for the soda-lime silicate glass was the complete opposite: only 3 of 17 tests were valid, including none of the etched specimens. For the unetched specimens, the strength was 1.7 GPa for both orientations, albeit with very few valid tests. We do not have a good explanation for why the success rate was so low for the soda-lime silicate glass.

Figure 2 shows the progression of damage in a representative specimen that failed in a valid manner. Initially, damage can be observed, but only in the gage section due to the flaws generated during the specimen machining process and higher stress in the gage section than the ends of the specimen. The flaws grow and coalesce, while the ends are still crack-free. Finally, complete structural collapse occurs in the middle of the gage section, with the ends subsequently fracturing as well. When the fracture was invalid, the cracks initiated at the specimen end(s) and propagated into the gage section. Figure 3 shows this fracture progression. Initially, surface roughness and cracks can be seen in the gage section due to light reflecting off the cracks. Then axial cracks are visible in the bottom section of the specimen, but there is no change in the damage located in the gage section. Next, axial cracks initiate and grow in the bottom of the specimen while the bottom portion of the specimen is expanding laterally, and additional damage is developing in the gage section. There is further lateral expansion of the bottom of the specimen, and complete structural collapse occurs.

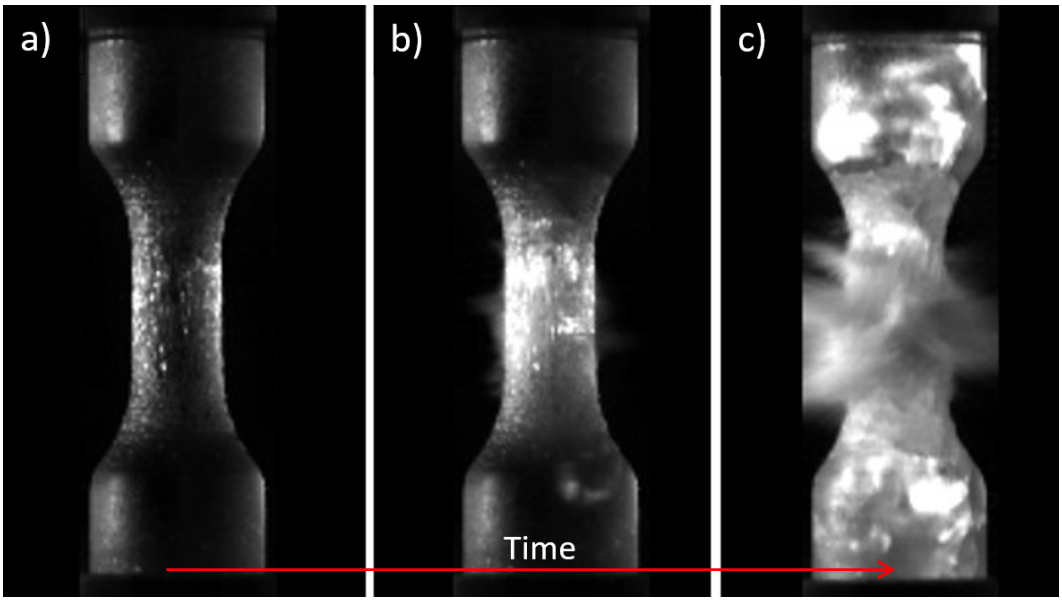


**Fig. 2 Fracture progression in a quasi-static specimen that yielded a valid result. a) Surface roughness from machining is observable in the gage section from the light reflecting off the features. b) Multiple cracks are forming and coalescing in the gage section. c) Load-carrying ability is lost, and complete structural collapse is evident. The time between the images is about 7 µs.**

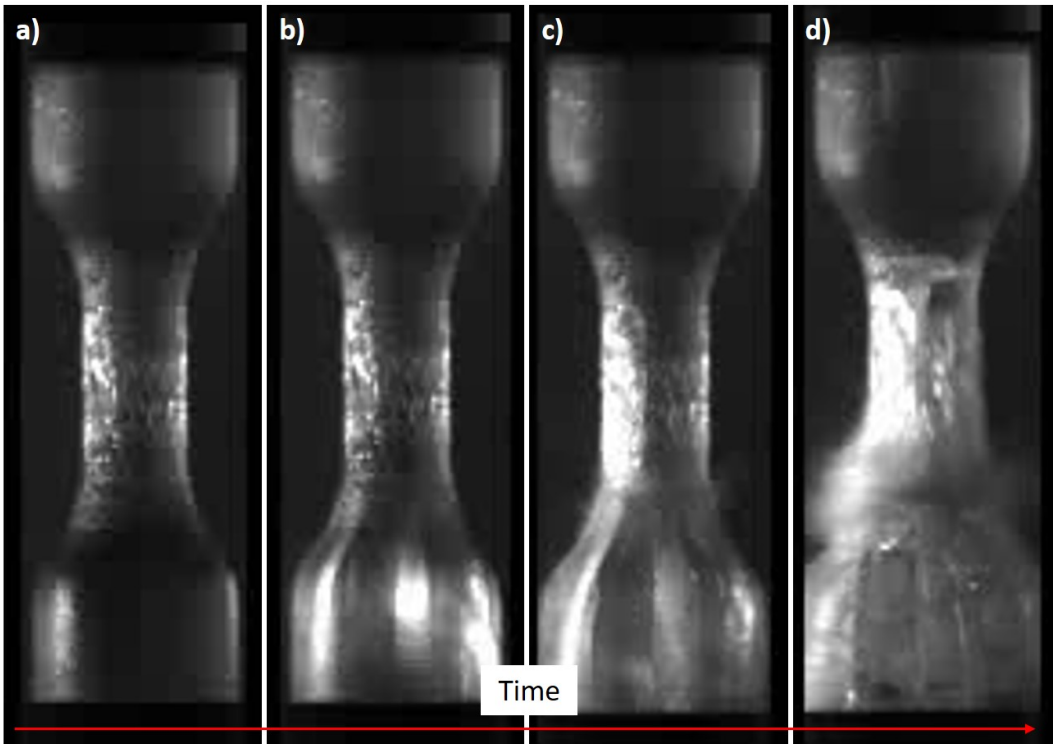


**Fig. 3 Fracture progression in a quasi-static specimen that yielded an invalid result. a) Surface roughness and cracks can be seen in the gage section. b) Axial cracks have formed in the bottom section of the specimen. c) Axial cracks continue to grow into the gage section. d) Complete structural collapse occurs. Time between images is about 6 µs.**

**Dynamic testing.** Table 2 summarizes the dynamic compression results for the high strain-rate tests. The horizontal specimens of both glasses were subjected to an HF etch, but the vertical specimens were not. The success rate for the borosilicate glass was 50% and the soda-lime glass was 0%. The validity of one of the etched borosilicate tests could not be classified because the camera did not trigger properly. The dynamic compression strength of the borosilicate glass is 1.7 ± 0.1 GPa, irrespective of the specimen orientation, whether the specimens were etched or not, or if a strain gage was mounted to the surface or not. This is slightly higher than the quasi-static strength results; however, there is a chance the three differences do have an effect but cancel out when all are changed at once, as was done in this work. Additionally, the three invalid specimens of the vertical, unetched borosilicate were "almost" valid, meaning that the initial signs of failure occurred in the gage section prior to cracks from the ends propagating in, but the time difference was so short that there was no coalescence of cracks in the gage section before the axial cracks came in from the specimen ends. However, the strength of all five vertical, unetched borosilicate specimens is 1.7 ± 0.1 GPa, which is statistically no different than considering only the valid specimens.

**Table 2 Dynamic compression strength results for borosilicate and soda-lime silicate glasses**

| Material | Direction | Unetched | | | | HF-Etched | | | |
|---|---|---|---|---|---|---|---|---|---|
| | | $\sigma_c$ (GPa) | StD | No. Specimens | Valid | $\sigma_c$ (GPa) | StD | No. Specimens | Valid |
| Borosilicate glass | Horizontal | . . . | . . . | . . . | . . . | 1.7 | 0.1 | 5[a] | 3 |
| | Vertical | 1.7 | 0.0 | 5 | 2 | . . . | . . . | . . . | . . . |
| Soda-lime glass | Horizontal | . . . | . . . | . . . | . . . | . . . | . . . | 5 | 0 |
| | Vertical | . . . | . . . | 5 | 0 | . . . | . . . | . . . | . . . |

[a] Validity unknown for one specimen

The lack of success testing the soda-lime silicate was disappointing, but it is consistent with the quasi-static results. The horizontal, etched specimens were all unambiguously invalid, usually with fracture initiating from both specimen ends almost simultaneously and propagating into the gage section. For the vertical, unetched soda-lime silicate specimens, a couple of tests were also almost valid. The failure strength of four of the specimens was 1.7 ± 0.2 GPa, where one was not considered for reasons discussed in the next paragraph. Therefore, there might be a difference in failure strength between the two directions or etched versus unetched, but more experiments would need to be performed to conclusively determine if this is the case.

The stress–time plots for the borosilicate and soda-lime glasses are shown in Figs. 4 and 5, respectively. Solid lines are valid tests, dashed lines are invalid, and the dotted line is unknown validity (due to a camera miss-trigger not capturing the fracture process). The time equal to zero for all the specimens corresponds to the chosen starting point of the transmitted wave (which stress is calculated from) used for analysis of the data. For most experiments, there is 5–10 μs where the specimens are essentially at zero stress. This is due to the geometry of the specimen, which is approximately 2.5× longer than a typical cubic or cylindrical specimen that would be used for the bar diameter used. Thus, it takes 2.5× longer for a wave to travel across the specimen, and because of the dumbbell shape more of the wave is reflected than would normally occur with a constant area specimen such as a cuboid or cylinder.

The consequence is that it takes many wave reverberations for a measureable amount of the wave to transmit into the transmitted bar. In other words, it takes several wave reverberations to build up a compressive force on the transmitted side of the sample. The compressive force builds up faster on the incident side, so it takes longer for the specimen to reach force equilibrium versus a typical cylindrical or cuboidal compression specimen. In the case of the soda-lime glass, a review of the high-speed video shows that axial cracking initiated in the end of the specimen in contact with the incident bar in 7 of the 10 invalid tests. This is probably the biggest disadvantage of using the dumbbell-shaped specimen in the Kolsky bar, where the loading times need to be relatively long and, thus, the strain rates will be relatively low. Compared with our previous work, there is significantly greater background noise with the strain-gage signals because a commercial strain-gage amplifier with a significantly higher bandwidth was used. The higher-bandwidth instrumentation was desired because of the shorter loading times in these tests. We chose not to filter/smooth the signals.

Both conditions of the borosilicate glass (Fig. 4) show consistent behavior, with failure occurring after about 30 μs. In graphical form, there is clearly no difference between the two specimen orientations or between valid versus invalid tests. For the soda-lime silicate glass, there is a greater test-to-test variation in the loading times, but there is no clear cause. Even though all of the specimens were invalid, there appears to be greater spread in the failure strengths, and the data show the possible strength difference between the horizontal etched and vertical unetched conditions. The extreme sawtooth-like shape of the V20 plot is likely due to a crack that formed in one of the transition sections (between the gage section and end) of the specimen very early in the loading, which can be observed in the high-speed images. The movement of this crack and/or the development of other cracks correlate to the erratic loading. It is possible there was a flaw present in the specimen that was not obvious prior to testing, or there could have been a misalignment in the Kolsky bar. Specimen V15 is starred in Fig. 5b

because there was a misfire with the Kolsky-bar gas gun, resulting in the sample being dynamically loaded to about 500 MPa but not failing the specimen. The specimen was subsequently tested, but there is no way to know if the inadvertent loading changed the subsequent behavior.

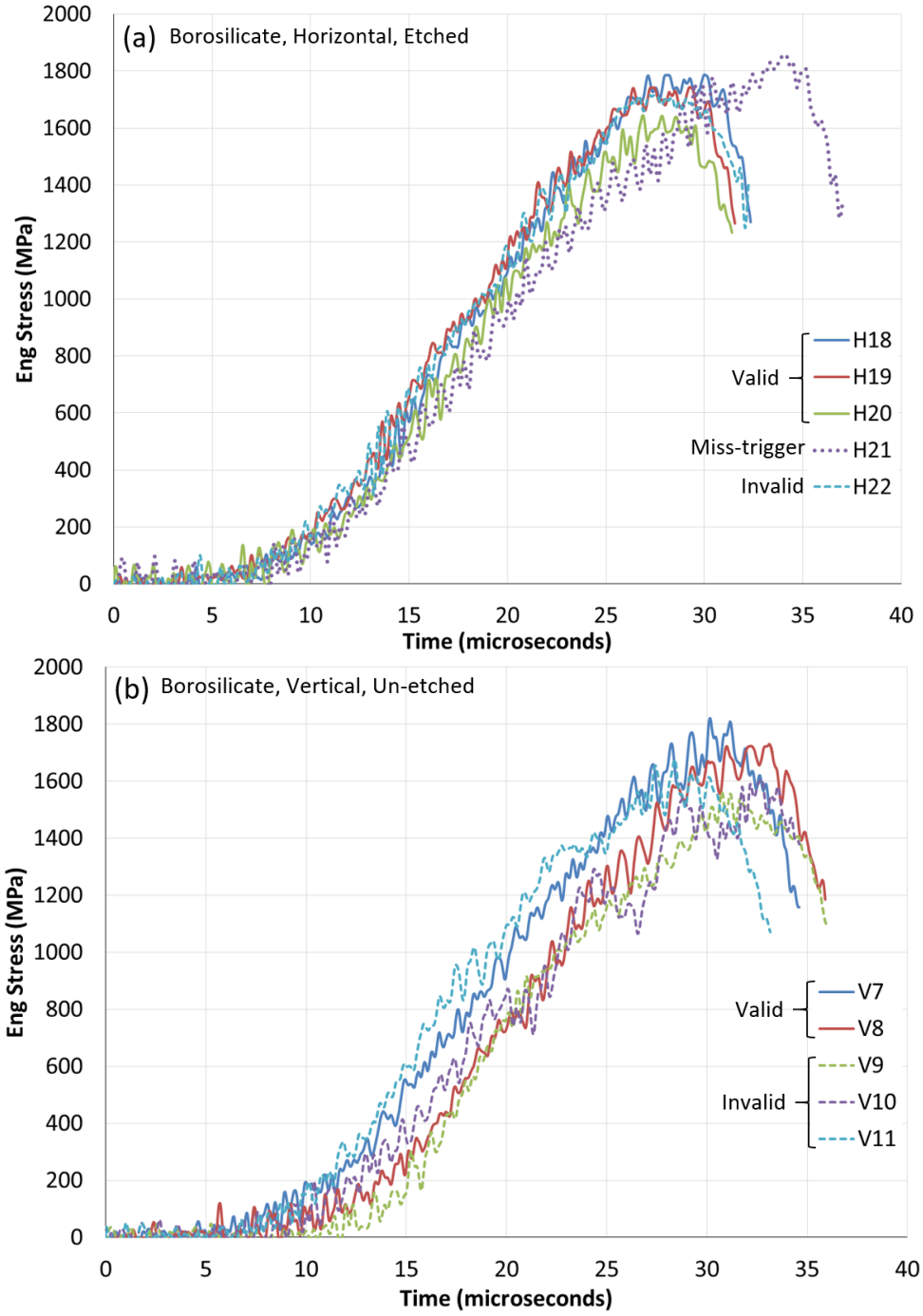


**Fig. 4 Dynamic compression loading of borosilicate in the a) horizontal direction, etched, and b) vertical direction, unetched**

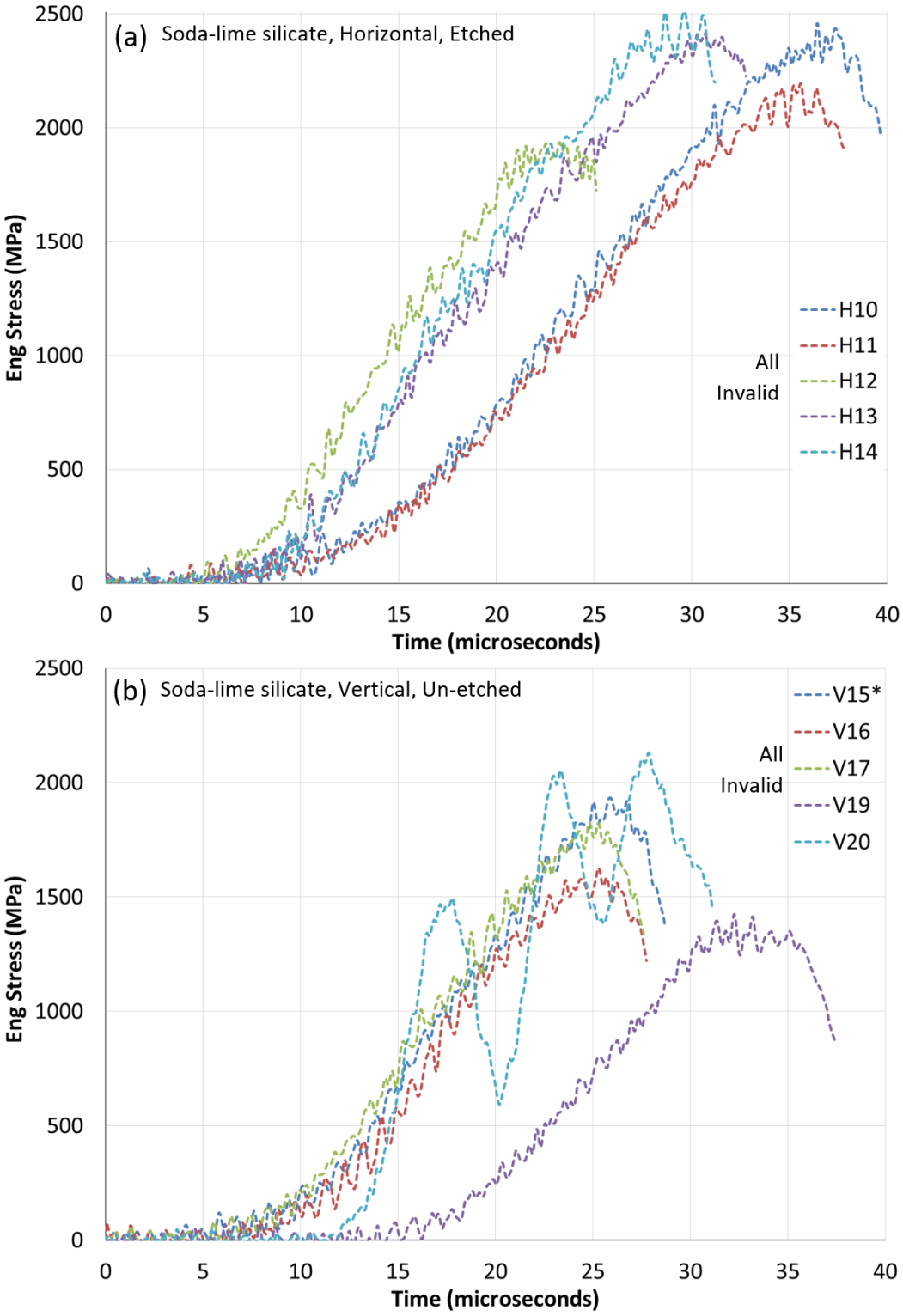


**Fig. 5 Dynamic compression loading of soda-lime silicate in the a) horizontal direction, etched, and b) vertical direction, unetched**

An example of damage evolution in one of the horizontal, etched borosilicate specimens that was valid is shown in Fig. 6. The stress–time plot is presented where the dots correspond to each indicated image. At 20 μs, there is no visible damage from the dynamic loading, but by 22 μs, an isolated spot has appeared. At 25.2 μs, the damage is propagating out from that initial location and additional damage has developed, and by 27.6 μs, the damage remains limited to the gage section. The peak stress of 1.6 GPa is not reached until about 28 μs. At this time, the damage encompasses most of the gage section but, importantly, only in the gage section. Just beyond the maximum stress, at 29.6 μs, axial cracks have propagated in from the transmitted end of the sample and load-carrying ability is lost. Thus, the cracks do not propagate in from the end(s) until after peak stress is reached.

Figure 7 shows a valid borosilicate specimen in the vertical, unetched condition. The first damage due to the dynamic loading conditions is visible at about 23 μs. By 27.5 μs, the damage is coalescing, but there are multiple disconnected regions of damage within the gage section. Additionally, the damage has a "ring"-like appearance, where the debris coming off the surface is constant about the circumference. At peak stress around 32 μs, the entire gage section is damaged, and cracks have already started to propagate in from the transmitted end (they first became visible at about 29 μs). Beyond about 33 μs, structural integrity is lost. Note the white area in the gage section visible at 20 and 23 μs is not damage but rather light reflected off of the underside of the strain gage mounted on the opposite face. This feature was present in the first image, which corresponds to the sample being essentially at zero load, and did not change throughout the loading until structural collapse. Similar features were visible and unchanging in the other unetched borosilicate samples with mounted strain gages.

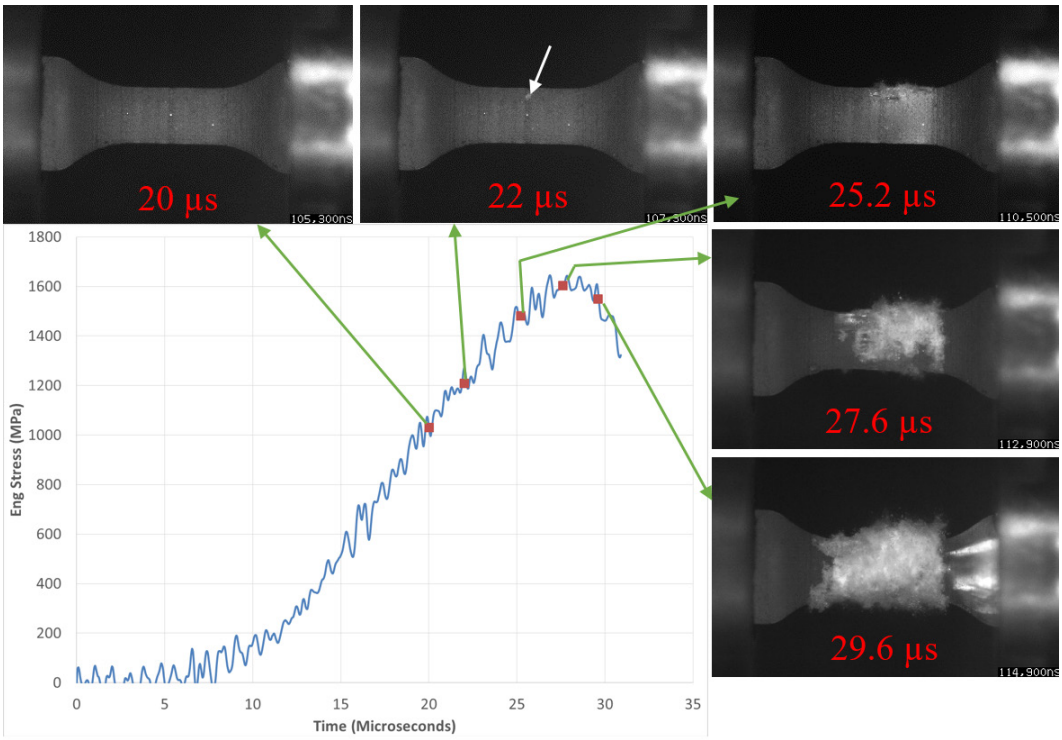


**Fig. 6 Borosilicate glass specimen H20, etched (valid); images with corresponding locations on the stress–time plot. The first visible damage occurs at 22 µs, with increasing damage beyond that until load-carrying ability is lost beyond ~29 µs.**

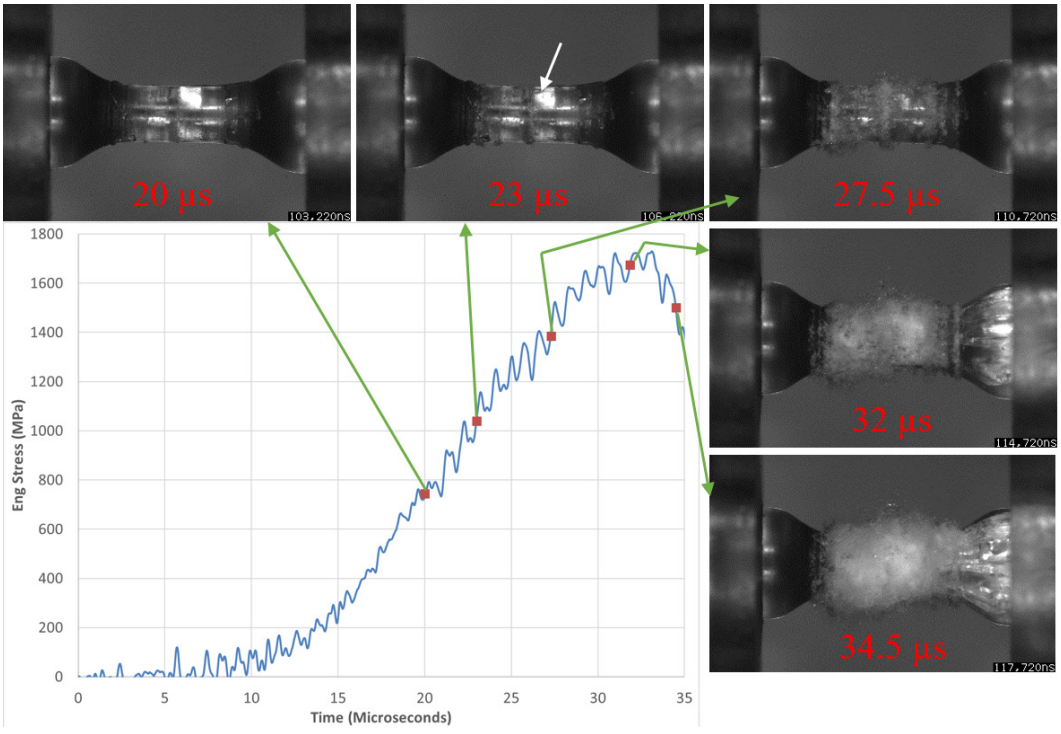


**Fig. 7 Borosilicate glass specimen V8, unetched (valid); images with corresponding locations on the stress–time plot. The first visible damage occurs at 23 µs, with increasing damage beyond that until load-carrying ability is lost beyond ~33 µs.**

Figure 8 shows an invalid test of soda-lime silicate in the vertical (unetched) direction. While considered invalid, it was "almost" valid (as mentioned before), and the failure was different from the previously mentioned conditions. At around 18 µs, damage starts appearing from multiple locations along the gage section simultaneously. At 21.6 µs, the damage has the appearance of the narrow, isolated "rings" that surround the gage section but they are better defined than with the borosilicate. Note there are visible ring-like striations within the gage section prior to visible damage, which correspond to marks made during the circumferential machining of the specimen. By the time peak stress occurs around 24.8 µs, cracks have already propagated in from the incident side and seem to be causing damage accumulation in the gage section. This is the main difference from the previous example and why this specimen was deemed invalid: The cracks from the end seem to be driving the structural collapse in the gage section, while in Fig. 7, structural collapse appears to originate from within the gage section itself. We admit that this is a subjective argument.

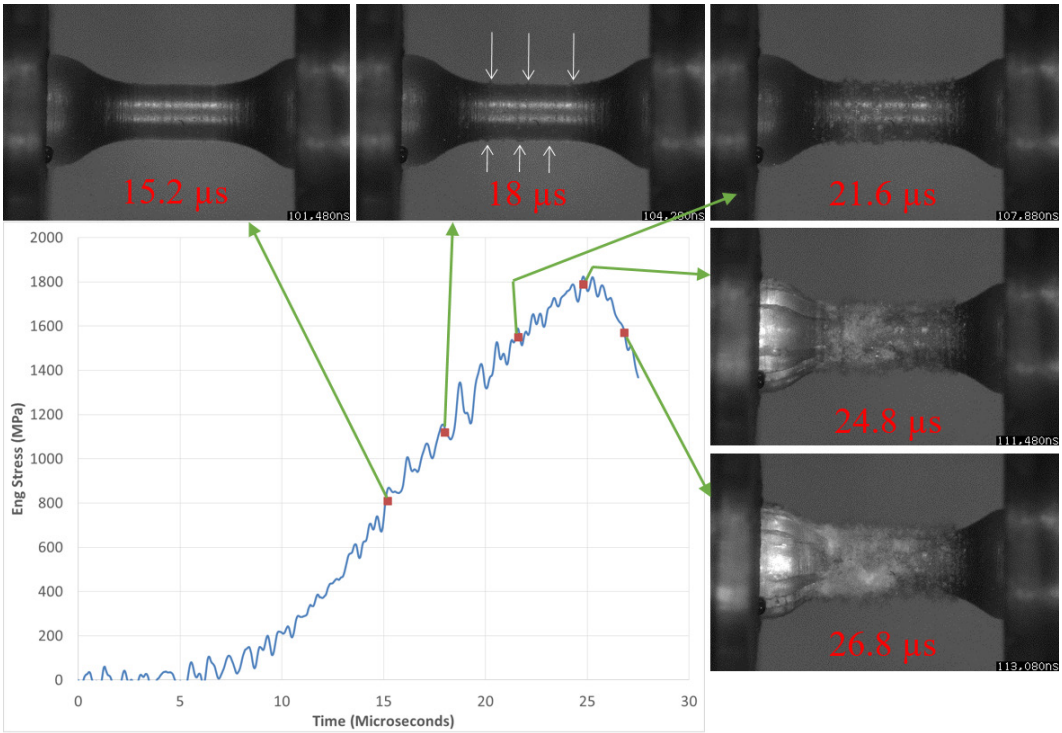


**Fig. 8 Soda-lime silicate glass specimen V17, unetched (invalid); images with corresponding locations on the stress–time plot. The first visible damage occurs at 18 µs, with increasing damage beyond that until load-carrying ability is lost beyond ~25 µs.**

## 5. Discussion

As mentioned in the Introduction, there are very few studies that measure the compression strength of glass, limiting the chances of a meaningful comparison. Figure 9 shows compression strength data from the literature for the same glasses (same brands).[14,16,20] Chocron et al.[14,16] performed unconfined and confined quasi-static compression experiments on cylinders of these materials and show three data points for the unconfined compression strength for each material. The strength of each of these specimens is indicated in Fig. 9. The soda-lime silicate and borosilicate had average strengths of 1.7 ± 0.4 and 2.0 ± 0.5 GPa, respectively. Chocron et al.'s average strength for soda-lime silicate under quasi-static conditions was the same as reported here, but the standard deviation is significantly higher. However, their borosilicate values are significantly higher, greater than one standard deviation, but it is unclear why. Another study, by Nie et al.,[20] measured the strength of borosilicate under Kolsky-bar loading using a cuboid specimen geometry to be 1.3 GPa (average of 10 tests and no standard deviation was reported), which is significantly less than the approximately 1.7 GPa measured in this study.

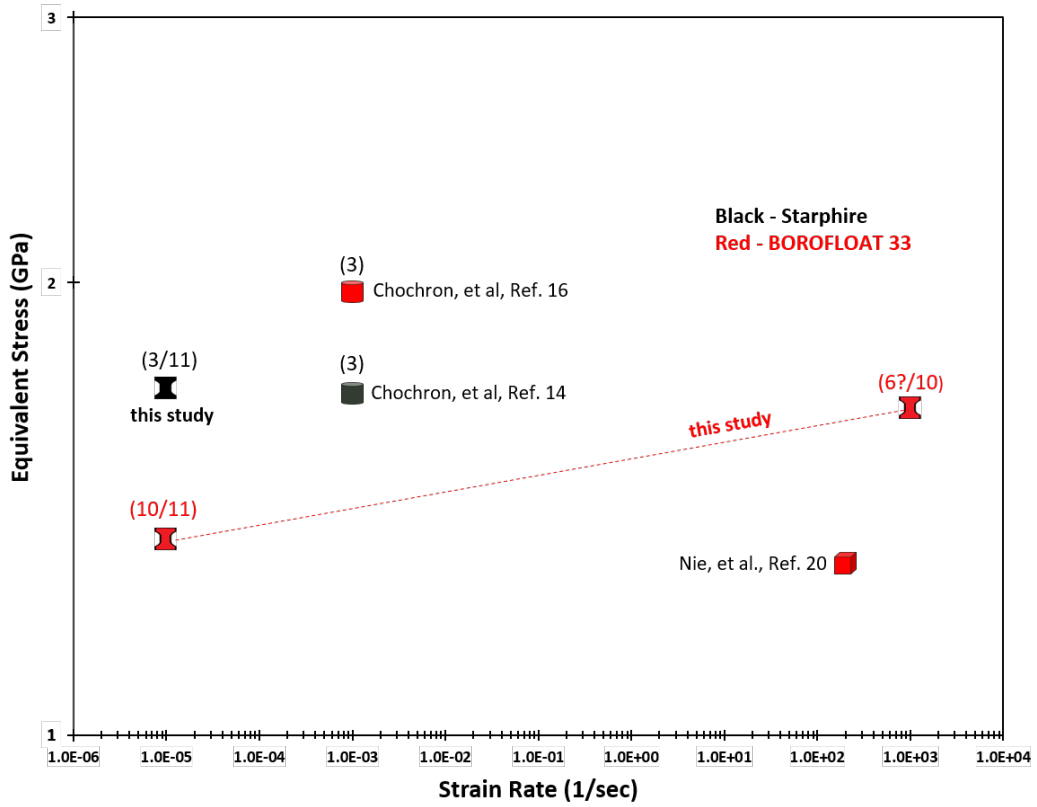


**Fig. 9 Compression strength as a function of applied strain rate (log–log plot) of borosilicate and soda-lime silicate glasses from this study generated using the dumbbell-shaped specimen and from others using cylinders[14,16] and cuboids[20]**

These results, taken together, indicate the standard deviation with the dumbbell-shaped specimen is significantly lower and a more accurate compression strength is measured than with cylinders or cubes. Finally, this is the first study where the strain-rate sensitivity of borosilicate glass can be assessed: The dynamic compression strength is about 20% higher than the quasi-static value. Recent work on $B_4C$ and alumina show no rate sensitivity and about a 30% increase, respectively, for this geometry. Traditionally, the standard deviations have been too large to determine if brittle materials are rate-sensitive and by how much. The strain-rate sensitivity of soda-lime silicate cannot be fully determined because no dynamic experiments were valid, but the average strength of the invalid experiments was slightly higher than the 1.7 ± 0.0 GPa for the valid quasi-static experiments, which hints that the glass may be strain-rate sensitive.

The paper by Nie et al.[20] also recorded the borosilicate sample fracturing, showing that initial fracture initiates from the end of the cubic specimen in contact with the Kolsky bar. This is significant evidence, along with the relatively low measured strength, that the stress concentration between the sample and Kolsky bar is leading to premature failure. Additionally, the initial sign of fracture does not correspond to the peak stress and is in accordance with this study. In Nie et al.'s example, initial failure occurs at approximately 1.3 GPa, while the peak stress occurs about 10 μs later at approximately 1.45 GPa. Examples from this study that exhibit a similar behavior are shown in Figs. 6 (Specimen H20) and 7 (Specimen V8). The initial indication of failure for H20 occurs at approximately 1.2 GPa, and peak stress occurs about 6 μs later at approximately 1.6 GPa. For V8, initial failure is at 1.05 GPa and peak stress is 9 μs later at approximately 1.7 GPa. Note the strain rate in this study was about 5× higher than in Nie et al. There are some differences in the stress and timing of the failures between the studies, but it is clear that peak stress does not correspond to the initial failure in the sample. The big difference is that in this study, initial failure occurs in the center of the gage section, while the previous study is at the edge of the sample. Thus, the dumbbell-shaped specimen allows for the discrimination of "valid" and "invalid" failures, whereas generally with cubes and cylinders, all experimental results are considered valid.

Determining test validity with this dumbbell geometry on glass can be subjective. A close examination of Figs 6–8 indicates why. Figure 6 shows that cracks from the end propagate toward the gage section after peak stress is reached, hence this experiment was deemed valid. However, we do not know when or where the cracks first initiated in the ends because the alignment collets hid this crack initiation from view. If cracks formed in the ends prior to peak stress, their presence could change the stress state within the gage section in such a way that promotes failure in the gage section. However, in Figs. 7 and 8, the cracks in the end are present prior to

reaching peak stress, but those experiments were deemed valid and invalid, respectively. One can argue that these should both be invalid tests, which certainly could be a convincing argument. However, we wanted the same validity criterion to be used for both quasi-static and dynamic tests: If appreciable damage occurs in the gage section prior to the appearance of cracks from the end(s), it is considered a valid test. In the authors' opinion, appreciable damage had occurred in the former but not the latter. The validity criterion has no mention of the presence of cracks with respect to the measured peak stress. For the quasi-static tests, the images recorded with the high-speed camera were not time-correlated to the measured force, so we could not compare the appearance of cracks propagating in from the end(s) with the load-displacement curve. Thus, for both quasi-static and dynamic experiments, validity was determined only by examining the high-speed videos of the fracture process.

Delaying the onset of failure in the ends or suppressing it altogether would reduce the subjective nature of determining validity. The most practical way to do this is to confine the ends to develop a net compressive stress when no axial load is applied. For glasses, heating a metal ring that cools and press-fits the ends may not be possible due to thermal shock. However, a press-fit can be achieved using a shaft collar, where tightening a screw tightens the internal diameter of the collar around each end. This also allows for control over the amount of tightening so that failure during tightening can be minimized. To ensure confining the ends does not induce stress in the gage section, strain gages can be adhered to the gage section, and any deviation from zero can be measured when tightening the collar.

In the future a less-subjective definition of what is valid or invalid could be implemented that states any cracks present outside the gage section have to initiate after the peak stress for the test to be valid. Such a change to the definition would require time-correlation with the force measurement, which is a significant challenge. Some events would have to be both visual—to be seen by the camera—and create a force signal "blip" that is readily identified. We know of no obvious method that currently exists. One possible solution would be to start recording force data and the images at the same time, but high-speed cameras often have limited memory and/or a limited number of images available at the required frame rates. It is also possible the force sensors in quasi-static load frames do not have sufficient bandwidth to accurately measure the true drop in the force signal, even if it was possible to perform a time-correlation.

Additionally, with Kolsky-bar experiments, there are additional uncertainties with time-synchronization between a high-speed camera and the strain gages because the strain-gage measurements are indirect: The sample has already fractured by the time the transmitted wave reaches the strain gage to be measured. In these

experiments, the camera and strain-gage data collection were triggered by the rise (in magnitude) of the incident wave, so the data shared a time equal to zero. However, there is uncertainty in the time for the waves to travel through the bars and specimen. As seen in Figs. 4 and 5, it takes several microseconds of wave reverberations through the specimen for measureable force to accumulate on the transmitted side of the specimen, so what should the chosen starting point of the transmitted wave be (from which specimen stress is calculated)? These uncertainties can easily add up to greater than a couple microseconds, which is a significant amount of time when the entire loading time was 25–30 μs for these experiments (depending on how it is defined). Increasing the loading time would reduce the uncertainty in the peak stress relative to obervations with high-speed video, but this would reduce the strain rate, which might not be desirable. Plus, failure is a process occuring over time, not a discreet event. The time difference between the appearance of the first evidence for fracture and when one can say structural collapse has occurred (from the images) is around several microseconds for the dynamic and maybe 3 to 4 times longer for the quasi-static loading. The loss of macroscopic-load-carrying ability could arguably occur at any point in that time period when one only observes the images. Adhering a strain gage to the gage section may reduce some error but is not a panacea. The failure of the material directly underneath the strain gage is not necessarily indicative of the loss of macroscopic-load-carrying ability. We fully admit our criterion is subjective; however, it is not clear there is a less subjective one to use.

An interesting aspect of the data in this effort is the difference in the success rate between borosilicate and soda-lime silicate glasses. The success rate of the former was 88% and 50% under quasi-static and dynamic loading, respectively. The success rate with the soda-lime silicate was 18% and 0% under quasi-static and dynamic loading, respectively. The reason for this is unknown. One factor could be the Poisson's ratio mismatch between the Kolsky bars and the samples, where each wants to expand radially by a different amount. However, the Poisson's ratios are close—0.180 for borosilicate versus 0.203 for soda-lime silicate, which seems too small of a difference to change the success rates between them that dramatically. Additionally, the quasi-static soda-lime silicate had valid experiments for the unetched condition, while the etched had none. This is counterintuitive because the etching was meant to reduce the surface damage caused by the specimen grinding. Since both conditions had low success rates, any differences introduced during etching does not seem to be the dominant reason for the material difference, especially when no effect was seen with the borosilicate. One thought is the grinding of the ends has a greater effect on axial crack formation in the soda-lime silicate relative to the borosilicate, but this is little more than a guess at this point, so we do not have a satisfactory explanation for the success rate difference.

Perhaps manufacturing the specimens using a method other than grinding (with or without etching) can give insight into the relative damage tolerance between the two glasses. Femtosecond laser machining has been used to machine 2-D and 3-D channels in glass for microfluidic applications, with feature sizes of approximately 10 μm to a few millimeters.[30–32] But it is unclear how the damage compares with this method versus traditional grinding used in this work. Also, making the cylindrical geometry of the dumbbell-shaped specimen at any size would be very challenging or impossible. Another possibility is to cast the samples directly into the dumbbell shape, thus eliminating the need for machining (although some machining may be required to obtain the tight tolerances). The complexity and cost of this option seems impractical, though. One possible avenue to improve the dynamic testing success rate with these glasses would be to use WC inserts between the glass specimen and the steel face of the test bars. The addition of WC inserts would slightly alter the wave propagation due to the impedance mismatch, but the higher elastic modulus of the WC, compared with the glasses, would provide some confinement of the glass surfaces at the WC–glass interface since the WC would not want to laterally expand as much as the glass, thus minimizing any tensile stress at this interface. WC platens were used during quasi-static testing and yielded a higher, but not significantly higher, success rate for achieving valid test results. Many of the invalid soda-lime silicate experiments with the Kolsky bar showed fracture initiating in the ends nearly simultaneously, potentially indicating that WC inserts would delay failure by reducing tensile stresses.

## 6. Summary and Conclusion

This report outlines the compression strength at quasi-static and dynamic strain rates of soda-lime silicate and borosilicate glasses using a dumbbell-shaped specimen. This specimen allows for an experiment to be deemed "valid" if failure occurs within the gage section and "invalid" if it initiates outside the gage section. For borosilicate glass at the quasi-static rate, the compression strength in the horizontal and vertical directions was 1.4 ± 0.1 and 1.3 ± 0.0 GPa, respectively, for the unetched specimens, and 1.5 ± 0.3 GPa for the etched specimens in the horizontal direction, where 17 of 19 experiments were valid. At the dynamic strain rate, the compression strength was 1.7 ± 0.0 GPa for vertical, unetched specimens and 1.7 ± 0.1 GPa for horizontal, HF-etched specimens, with 5 of 10 experiments valid. The soda-lime silicate glass, on the other hand, had a significantly lower success rate at both strain rates: for the horizontal unetched, two of eight were valid (1.7 ± 0.0 GPa); for the vertical unetched, one of four were valid (1.7 GPa); and for the HF-etched in both directions, zero of the 10 were valid. The dynamic experiments also had a zero of 10 success rate for vertical, unetched, and horizontal

HF-etched. We could not identify a cause for the dramatically different success rates between the two glasses. While compression strength data on these materials in the literature are very sparse, the dumbbell-shaped specimen results in a significantly lower standard deviation and allows one to discriminate between valid and invalid results, which is not possible with typical cubic and cylindrical geometries, where every experiment is generally valid. The lower standard deviation also allows strain-rate effects to be determined.

However, these experiments show that determining validity is not as straightforward as the simple description provided previously. Usually specimens fractured with initial damage occurring within the gage section, but cracks propagated in from the ends as the gage section was failing. This adds ambiguity and subjectiveness to the validity determination that is not easily avoided. Time correlating the force measurement to the high-speed video images showing failure is helpful, but there are uncertainties with this, especially at dynamic rates with the Kolsky bar where the force measurement is indirect.

## 7. Future Work

It is clear from this effort that additional testing needs to be conducted to generate a representative compression strength value for glasses and increase the success rate for obtaining valid test results. Some of this may include the following:

- Improved methods for machining the dumbbell-shaped specimens to minimize the development of cracks at the surface
- Optimization of HF etch of machined specimens to significantly reduce or eliminate the machining-induced cracks
- Manufacture dumbbell-shaped glass specimens directly to eliminate the need for machining
- Use of sacrificial WC platens to minimize lateral expansion of the glass at the interface between the end of the specimen and the load platen
- Place the ends of the dumbbell specimens under compression using a confinement process to reduce the likelihood of cracks initiating in this location

## 8. References


1. ASTM C158-02. Standard test methods for strength of glass by flexure (determination of modulus of rupture). ASTM International; 2012.
2. ASTM C1499-09. Standard test method for monotonic equibiaxial flexural strength of advanced ceramics at ambient temperature. ASTM International; 2009.
3. Swab JJ, Thies S, Wright JC, Schoenstein J, Patel P. Influence of surface scratches on the flexure strength of soda-lime-silicate and borosilicate glass. Exper Mech. 2016;53(1):91–96.
4. Swab JJ, Patel PJ, Tran X, Gilde L, Luoto E, Gaviola MH, Gott A, Paulson B, Kilczewski S**.** Equibiaxial flexure strength of glass: influence of glass plate size and equibiaxial ring ratio. Int J Appl Glass Sci. 2014;5(4):384–392.
5. Cachairas A, Gilde L, Swab JJ, Patel PJ, Quinn GD. Soda-lime-silicate float glass: a property comparison. Army Research Laboratory (US); 2017 Oct. Report No.: ARL-TR-8187.
6. Bridgman PW. Reflections on rupture. J App Phys. 1938;9(8):517–528.
7. Bridgman PW. The effect of hydrostatic pressure on the fracture of brittle substances. J App Phys. 1947;18(2):246–258.
8. Bridgman PW, Simon I. Effects of very high pressures on glass. J App Phys. 1953;24(4):405–413.
9. Outwater JO, Gerry DJ. The effects of high uniaxial compressive stress on glass. Naval Research Laboratory (US); 1966. Contract No.: NONR 3219 (01)(X).
10. Outwater JO, Gerry DJ. Effects of high uniaxial compressive stress on glass. J App Phys. 1967;38:893–894.
11. Ernsberger FM. Tensile and compressive strength of pristine glasses by an oblate bubble technique. Phys Chem Glass. 1969;10(6):240–245.
12. Moreno DH, Silva ML. The effects of size and environment on the uniaxial compressive breaking strength of glass, alumina and pyroceram. Naval Ship Research and Development Center (US); 1970. Report No.: 3315.
13. Danneman KA, Chocron S, Nicholls AE, Anderson Jr CE. Compressive damage development in confined borosilicate glass. Mat Sci Eng A. 2008;478:340–350.

14. Chocron S, Anderson Jr CE, Nicholls AE, Dannemann KA. Characterization of confined intact and damaged borosilicate glass. J Am Ceram Soc. 2010;93(10):3390–3398.

15. Danneman KA, Anderson Jr CE, Chocron S, Spencer JF. Damage development in confined borosilicate and soda-lime glass. J Am Ceram Soc. 2012;95(2):721–729.

16. Chocron S, Anderson Jr CE, Dannemann KA, Nicholls AE. Pressure effects on the compressive response of confined intact and damaged soda-lime glass. Exp Mech. 2013;53:77–89.

17. Peroni M, Solomos G, Pizzinato V, Larcher M. Experimental investigation of high strain-rate behavior of glass. App Mech Mat. 2011;82:63–68.

18. Zhang X, Zou Y, Hao H, Li X, Ma G, Liu K. Laboratory test on dynamic material properties of annealed glass. Int J Protect Struct. 2012;3(4):407–430.

19. Daryadel SS, Mantena PR, Kim K, Stoddard D, Rajendran AM. Dynamic response of glass under low-velocity impact and high strain rate SHPB compression loading. J Non-Cry Solids. 2016;432:432–439.

20. Nie X, Chen WW, Sun X, Templeton DW. Dynamic failure of borosilicate glass under compression/shear loading experiments. J Am Ceram Soc. 2007;90(8):2556–2562.

21. Tracy CA. A compression test for high strength ceramics. J Test Eval. 1987;15(1):14–19.

22. Tracy CA, Slavin M, Viechnicki D. Ceramic fracture during ballistic impact. In: Frechette VD, Varner JR, editors. Fractography of glasses and ceramics. Advances in ceramics. Vol. 22. American Ceramic Society; 1988. p. 295–306.

23. Dunlay WA, Tracy CA, Perrone PJ. A proposed uniaxial compression test of high strength ceramics. Army Materials Technology Laboratory (US); 1989. Report No.: TR 89-89.

24. Blumenthal WR, Gray GT III, Claytor TN. Response of aluminum-infiltrated boron-carbide cermets to shock-wave loading. J Mat Sci. 1994;29:4567–4576.

25. Swab JJ, Meredith CS, Casem DT, Gamble WR. Static and dynamic compression strength of hot-pressed boron carbide using a dumbbell-shaped specimen. J Mat Sci. 2017;52:10073–10084.

26. Swab JJ, Quinn GD. Dynamic compression strength of ceramics: results from an interlaboratory round-robin exercise. Army Research Laboratory (US); 2019 Nov. Report No.: ARL-TR-8860.

27. Weresczcak AA, Anderson CE Jr. Borofloat and starphire float glasses: a comparison. Int J Appl Glass Sci. 2014;5(4):334–344.

28. ASTM C1424-15. Standard test method for monotonic compression strength of advanced ceramics at ambient temperature. ASTM International; 2016.

29. Vishay Precision Group. Instruction bulletin B-129-8; 2011 Dec 19. https://micro-measurements.com/knowledge-base/instruction-bulletins.

30. Giridhar MS, Seong K, Schülzgen A, Khulbe P, Peyghambarian N, Mansuripur M. Femtosecond pulsed laser micromachining of glass substrates with application to microfluidic devices. Appl Optics. 2004;43(23):4584–4589.

31. Mačernyte L, Skruibis J, Vaičaitis V, Sirutkaitis R, Balachninaitė O. Femtosecond laser micromachining of soda-lime glass in ambient air and under various aqueous solutions. Micromachines. 2019;10:354.

32. Sugioka K, Cheng Y, Midorikawa K. Three-dimensional micromachining of glass using femtosecond laser for lab-on-a-chip device manufacture. Appl Phys. 2005;A(81):1–10.

## List of Symbols, Abbreviations, and Acronyms

| | |
|---|---|
| 2-D | two-dimensional |
| 3-D | three-dimensional |
| $B_4C$ | boron carbide |
| HF | hydrofluoric acid |
| WC | tungsten carbide |

1 (PDF) DEFENSE TECHNICAL INFORMATION CTR DTIC OCA

1 (PDF) DEVCOM ARL FCDD RLD DCI TECH LIB

86 (PDF) DEVCOM ARL
FCDD RLR
D STEPP
FCDD RLR E
C VARANASI
FCDD RLR EM
M BAKAS
E RUNNERSTROM
FCDD RLW
A RAWLETT
S SCHOENFELD
J ZABINSKI
FCDD RLW B
C HOPPEL
R BECKER
J CAMPBELL
P GILLICH
A TONGE
L VARGAS-GONZALEZ
FCDD RWL D
B MCWILLIAMS
FCDD RLW LH
D D MALLICK
L MAGNESS
P A JANNOTTI
FCDD RLW P
J D HOGGE
FCDD RLW PC
A D BROWN
C A GUNNARSSON
J R MCDONALD
S S SATAPATHY
T WEERASOORIYA
FCDD RLW PC
D T CASEM
J U CAZAMIAS
J D CLAYTON
R B LEAVY
J T LLOYD
C S MEREDITH
T W SCHARF
L S SHANNAHAN
S TURNAGE
C L WILLIAMS
FCDD RLW PD
R DONEY
K STOFFEL
M B ZELLNER
FCDD RLW PE
C KRAUTHAUSER
P SWOBODA
FCDD RLW S
J CIEZAK-JENKINS
A WEST
FCDD RLW M
B CHEESEMAN
E CHIN
K CHO
W ROY
FCDD RLW MA
J SANDS
E WETZEL
FCDD RLW MB
C FOUNTZOULAS
G GAZONAS
J LIGDA
B LOVE
D MAGAGNOSC
J PITTARI
B POWERS
J SIETINS
Z WILSON
FCDD RLW MC
S WALCK
FCDD RLW MD
J LA SCALA
S WALSH
FCDD RLW ME
K BEHLER
V BLAIR
R BRENNAN
S COLEMAN
A DIGIOVANNI
J DUNN
M GOLT
M GUZIEWSKI
S HIRSCH
C HUBBARD
M IVILL
M KORNECKI
N KU
J LASALVIA
T PARKER
P PATEL
S RAJU
A ROSENBERGER
W SHOULDERS
S SILTON
J SWAB
FCDD RLW MF
P GOINS
C HAINES
E HERNANDEZ
E HORWATH

FCDD RLW MG
J LENHART
R MROZEK
E NAPADENSKY

5 DEVCOM SC
(PDF) FCDD SCP
J KIREJCZYK
FCDD SCP WI
R DILALLA
A FOURNIER
C LEWIS
FCDD SCP WP
D PHELPS

1 SFAE SDR SPIE
(PDF) D OTTERSON